Recent Data of Extensive Air Showers Recorded by Alborz I Array and Their Detailed Analysis

Mahmud Bahmanabadi[*1] · Mostafa Heydarizad[2]

1   Department of Physics, Sharif University of Technology, PO Box 11155-9161, Tehran, Iran;
    *email: bahmanabadi@sharif.edu
2   Alborz Observatory, Sharif University of Technology, PO Box 11155-9161, Tehran, Iran;
    email: heydarizadmustafa@gmail.com

Abstract. An array of five scintillation detectors has been installed in Sharif University of Technology to record extensive air showers. By using the time lags of the secondary particles of air showers relative to each other and the location of each of these particles relative to the core of the shower, the arrival direction of the primary particle producing each air shower has been obtained. These data show that the distribution of time intervals of successive events in all directions of arrival into the atmosphere is a random distribution. The distribution of the time intervals between successive events in different seasons has also been obtained and the seasonal effect has been investigated. The effects of the environment, including temperature and pressure, on the cosmic ray count rate have been investigated. The distribution of zenith and azimuth angles, as well as the solar, sidereal, and antisidereal time distributions of cosmic rays, have been obtained.

Keywords: Cosmic Rays, Extensive Air Shower, Random Events

1   Introduction

Cosmic rays are energetic particles and nuclei of various elements whose energy spectrum falls sharply with a power law, ranging from a few Megaelectron-volts (MeV) to about Zettaelectron-volts (10^{21}eV) per particle. Low-energy primary cosmic rays due to their high flux can be directly measured by satellite or balloon experiments. Primary cosmic rays interact with atmospheric molecules to produce secondary particles that can be detected on Earth's surface. At high energies, secondary particles produced (extensive air shower) by a single primary particle can be detected. These showers can be reconstructed to determine the energy, direction and composition of the incident particles. In this paper, by recording cosmic rays with an array of 5 scintillator detectors, we have investigated in detail the statistical distribution of their counting with the theory of random events. The effects of weather, including temperature and air pressure, on cosmic ray count rate are studied. Their zenith and azimuth distributions, and also solar, sidereal, and antisidereal time distributions are investigated.

2   Array layout

Figure 1 shows a demonstration of a small array including 5 scintillation detectors which is considered as experimental setup. The geometry of this array is arranged as a regular pentagon with a side length of 5 meters. As shown in Figure 1, the detectors are numbered

from 1 to 5, respectively. The direction of the magnetic north relative to the detectors is indicated by the letter N. Each detector consists of a 50cm×50cm×2cm scintillation slab which is housed in a light enclosure with a shape of a regular pyramid and a height of 20 cm. This height has been optimized for the light enclosure in our previous work [1]. At the top of each pyramidal light enclosure is installed a photomultiplier tube with a diameter of 5 cm (PMT, 9813B). The details of each detector are demonstrated on the left side of Figure 1. An event is recorded when different particles of an air shower pass through the five detectors. The electronic circuit used (Figure 1) is such that the time difference of the particles passing through the detectors 2 to 5 from the detector 1 are measured. The passage of each particle through each detector generates a signal in the respective photomultiplier. Signal of each PMT is connected to the input of one of the channels of an 8-channel fast discriminator (CAEN N413A). All channels of the fast discriminator are in a -20 mV threshold level. The output of the discriminator channel associated with the detector #1 is connected to the start inputs of the four Time to Amplitude Conveter (TAC) modules. The outputs of the other discriminator channels which are related the detectors #2 to #5 connect to the stop inputs of the same four TACs. The stop inputs are accompanied by a time delay using additional cables. And in the final step, the outputs of the four TACs (which all are set with a time window 200 ns) are connected to a Multi-Channel Analyzer (MCA) through an Analog to Digital Converter (ADC, KIAN AFROUZ Inc.) unit. Meanwhile, the output of TAC #1 acts as a gate signal for data recording.

3   Analysis of recorded time data

Our air shower array is located at Sharif University of Technology, Tehran, Iran (latitude $35°43'$ N, longitude $51°20'$E) at an altitude of 1200 m = 897 gcm^{-2}. During almost one year, 564763 EAS events in zenith angle between $0°$ and $60°$ and all azimuth angles, and in the energy range between 30 TeV and 3000 TeV [2] were collected. The total observation time was 5133 hours and hence the trigger rate was approximately $r \simeq 1.8$ events/min. Two sets of time data are available from the array. One is the time difference between the secondary particles of each shower passing through the different detectors, and another is the recording time of each air shower by the array. We study each of these two time datasets which contain some of the characteristics of the cosmic rays and the related air showers parameters. We use the first data to determine the arrival direction of cosmic rays into the atmosphere, and the second data to determine the distribution of time intervals between them, and also the distributions of solar and sidereal times.

3.1   Method of obtaining air shower direction and analysis

We assume that the air shower front is a plane surface with a normal vector along the shower axis, and direction of each air shower, using the time lags between the detector No.1 and the rest of the detectors is calculated. As shown in Figure 2, when the shower axis (which is perpendicular to the shower plane) hits the ground along $-\hat{n}$, the time difference between the arrival of the shower front at point $\vec{x}_i$ (on the ground) and the reference point $\vec{x}_r$ (detector No.1) is as follows

$$t_i - t_r = -\frac{1}{c}\hat{n}.(\vec{x}_i - \vec{x}_r), \tag{1}$$

where it is assumed that all particles move at the speed of light, c, and the unit vector $\hat{n}$ in terms of the zenith, θ, and azimuth, φ, angles is ($\sin\theta\cos\varphi$, $\sin\theta\sin\varphi$, $\cos\theta$).

The azimuth angle, φ, is measured in the direction of movement from the magnetic north
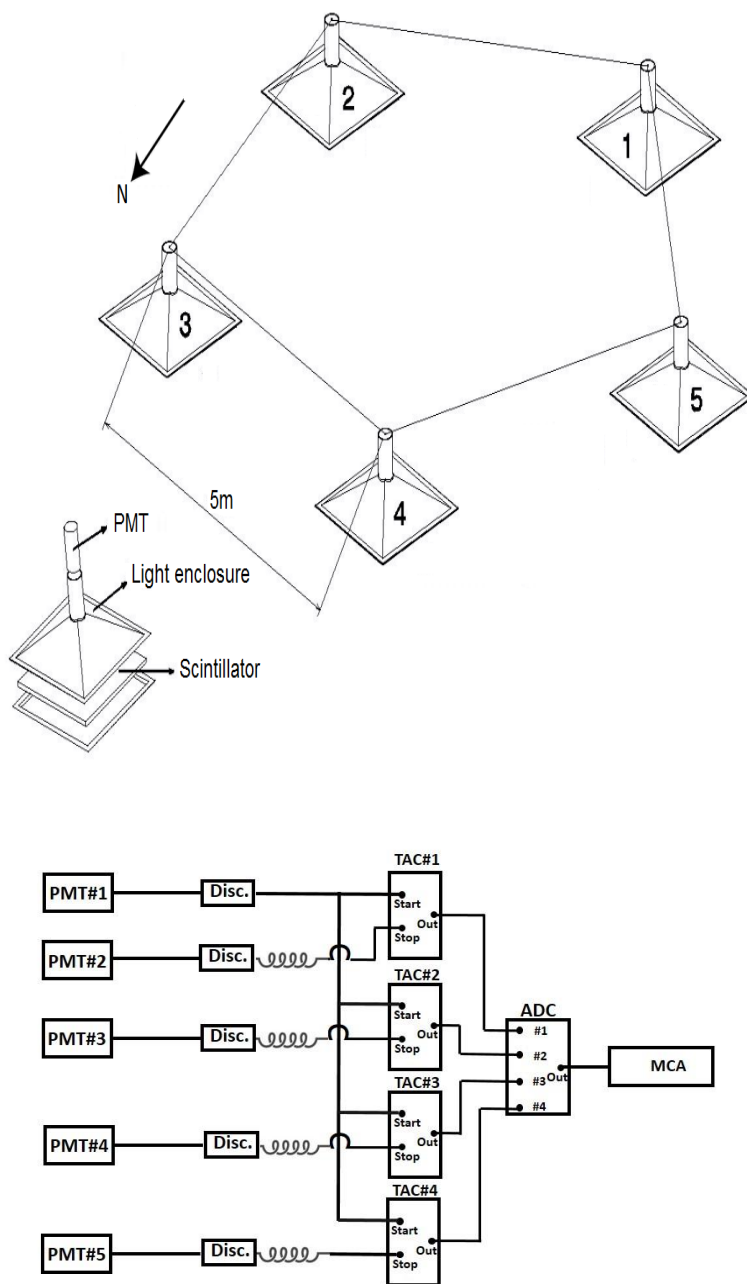
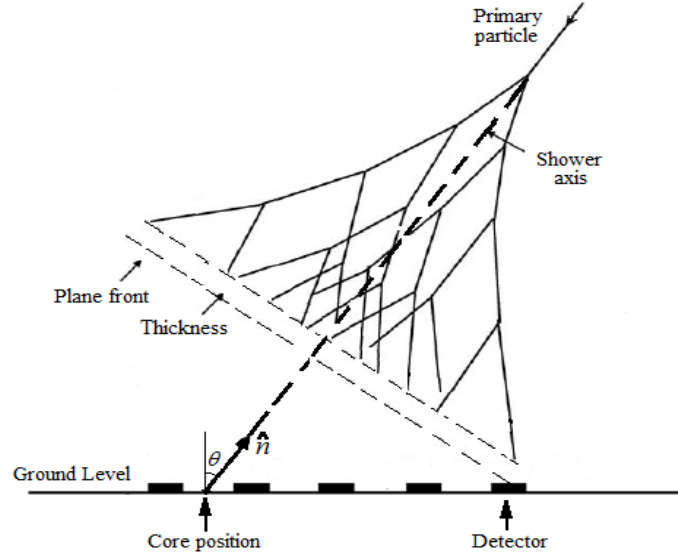Figure 1: Array layout and electronic circuits.

Figure 2: Schematic of shower front geometry, shower axis, and arrival angle of shower.

counter-clockwise. In other words, $\varphi = 0$ points to the magnetic north, and the direction of movement is to the west. To find the directional angles (θ, φ) of a shower, we minimize the sum of squares of the time differences between the measured data and the model (Equation 1) time prediction, that is, the following function, χ^2, is minimized.

$$\chi^2 = \sum_i [c(t_i - t_r) + \hat{n}.(\vec{x}_i - \vec{x}_r)]^2. \tag{2}$$

By writing the station coordinates as $\vec{x}_i = (x_i, y_i, z_i=0)$, and the reference coordinates (detector No.1) as $\vec{x}_r = (0, 0, 0)$, we have

$$\chi^2 = \sum_i [c(t_i - t_r) + x_i \sin\theta \cos\varphi + y_i \sin\theta \sin\varphi]^2. \tag{3}$$

To minimize χ^2, we define $u = \sin\theta \cos\varphi$ and $v = \sin\theta \sin\varphi$ and have

$$\frac{\partial \chi^2}{\partial u} = 2 \sum_i x_i [c(t_i - t_r) + x_i u + y_i v] = 0,$$

$$\tag{4}$$

$$\frac{\partial \chi^2}{\partial v} = 2 \sum_i y_i [c(t_i - t_r) + x_i u + y_i v] = 0.$$

So u and v are solved as follows

$$u = \frac{w_3 w_5 - w_2 w_4}{w_1 w_2 - w_3^2}, \qquad v = \frac{w_3 w_4 - w_1 w_5}{w_1 w_2 - w_3^2}, \tag{5}$$

where

$$w_1 = \sum_i x_i^2, \qquad w_2 = \sum_i y_i^2, \qquad w_3 = \sum_i x_i y_i,$$

$$w_4 = c \sum_i x_i(t_i - t_r), \qquad w_5 = c \sum_i y_i(t_i - t_r).$$

Finally, θ and φ are obtained from the following relations

$$\sin\theta = \sqrt{u^2 + v^2}, \qquad \tan\varphi = \frac{v}{u}. \tag{6}$$

Using this method, the direction of each shower, θ and φ, is calculated with the data of the pentagon array in Figure 1. In fact, the time delays between four detectors (No.2, 3, 4, and 5) and the detector No.1, along with the location coordinates of the four detectors relative to the detector No.1 are used to determine the values of w_1 to w_5. Then, using equation (6), θ and φ values were obtained. The distribution function of the zenith angle, theta, is shown in Figure 3. This distribution can be represented by the function $dN = N_0 \sin\theta \cos^m\theta \, d\theta$. By fitting this function on the distribution obtained from the array data, the value of $m = 7.2\pm0.1$ is obtained, which is in good agreement with the performed simulation [3].
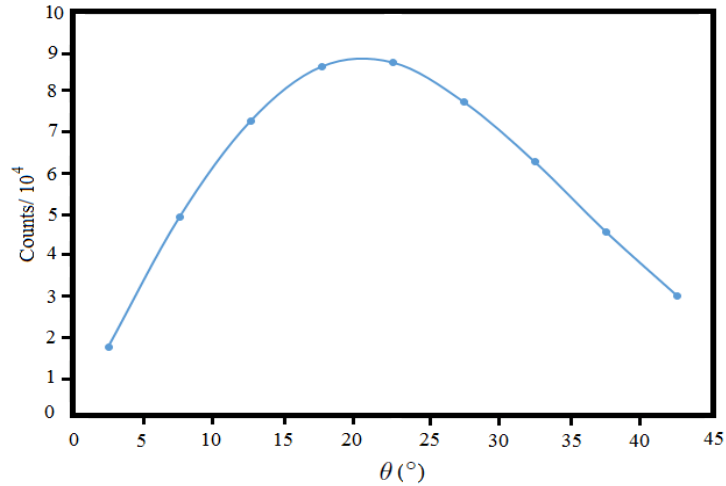

Figure 3: Distribution of zenith angle of air showers, θ.

The azimuth distributions of recorded air showers is also shown in Figure 4. These distributions were obtained in three zenith angle intervals, $0° - 15°$, $15° - 30°$, $30° - 45°$, and $\theta \le 45°$. These distributions are represented by Fourier analysis (up to the first harmonic) as

$$N(\varphi_i) = N_0 + N_1 \cos(\varphi_i - \varphi) = N_0 + N_1 \cos\varphi \cos\varphi_i + N_1 \sin\varphi \sin\varphi_i. \tag{7}$$

The azimuth angle is divided by the bin width of 20 degrees. Hence, $N(\varphi_i)$ is the number of cosmic rays in the interval $(20i - 20)° \le \varphi_i < (20i)°$; $i = 1, 2, 3, \dots, 18$. The Fourier coefficients $a = N_1 \cos\varphi$ and $b = N_1 sin\varphi$ with first harmonic analysis in terms of azimuth
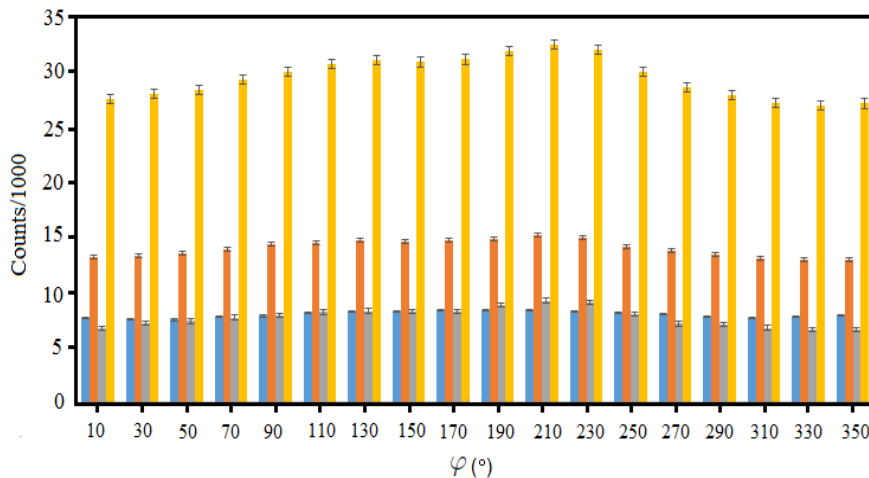
Figure 4: Distribution of the number of air showers in azimuth angles, in different zenith angle intervals. In each bin, the boxes from left to right show the number of events in the zenith angle intervals 0°-15°, 15°-30°, 30°-45° and $\theta \leq 45°$ respectively.

angle are as follows

$$a = \frac{2}{k}\Sigma_{i=1}^{k}N(\varphi_i)\cos\varphi_i, \qquad b = \frac{2}{k}\Sigma_{i=1}^{k}N(\varphi_i)\sin\varphi_i. \qquad (8)$$

Here, k=18 and $\varphi_i = (20i - 10)°$. The mean value of $N(\varphi_i)$, and the amplitude and phase of the first-harmonic modulation are given by $N_0 = \frac{1}{k}\Sigma_{i=1}^{k}N(\varphi_i)$, $N_1 = \sqrt{a^2 + b^2}$, and $\varphi = \arctan(b/a)$ respectively. Nonuniformities effects are accounted with the normalization factor N_0, that is, with the fractional amplitude $f = N_1/N_0 = \sqrt{a^2 + b^2}/N_0$. The Rayleigh analysis for the probability to obtain an amplitude larger than the one measured as a result of a fluctuation from an isotropic distribution is given by $P(\geq f)$=$\exp(-\mathcal{N}f^2/4)$. Where $\mathcal{N}$ is the number of events used in the data set. For each zenith bin, we report in Table 1 the number of events $\mathcal{N}$, the amplitudes N_0, and N_1, the first harmonic phase φ, and the chance probability $P(\geq f)$. One can see that the first harmonic modulation in the azimuth angle leads to the fractional amplitude of f=0.082 ±0.001 for $\theta \leq 45°$, which can be generated by Rayleigh analysis with probability almost zero from an isotropic distribution. The phase of the maximum of this modulation is a ϕ=171°±10°, indicating an effect of north–south anisotropy. The anisotropy in the azimuth angle distribution depends on the geomagnetic location of the observatory, the energy and electric charge of the primary particles. Particles coming from the north, due to being perpendicular to the magnetic field lines, suffer more deviation than the particles coming from the south. Therefore, the efficiency of recording showers from the south is greater than from the north. To estimate this anisotropy, the total number of event counts from the southern half-space, N_s, is compared with the northern half-space, N_n. By defining the amplitude of anisotropy as $2(N_s - N_n)/(N_s + N_n)$, and its error as $4(N_sN_n)^{0.5}/(N_s + N_n)^{1.5}$, the values of $(6.4 \pm 0.3)\%$, $(8.6 \pm 0.2)\%$, $(16.0 \pm 0.3)\%$, and $(9.9 \pm 0.1)\%$ are obtained for zenith angle intervals of $0° - 15°$, $15° - 30°$, $30° - 45°$, and $\theta \leq 45°$ respectively. One can see that as the zenith angle increases, the anisotropy increases, indicating a larger effect of the geomagnetic field on the longer path of charged particles in the atmosphere.

Table 1: Fourier amplitudes and phases at the azimuth angles, and the Probabilities to get larger values from statistical fluctuations of an isotropic distribution for three zenith angle intervals.

zenith angle	$\mathcal{N}$	N_0	N_1	$f(\%)$	$\varphi(°)$	$P \geq f$
$0° - 15°$	140415	7801	367	4.7 ± 0.2	188 ± 10	2.1×10^{-34}
$15° - 30°$	252801	14045	1008	7.2 ± 0.2	170 ± 10	5.0×10^{-142}
$30° - 45°$	139578	7754	1048	13.5 ± 0.4	173 ± 10	1.8×10^{-277}
$\theta \leq 45°$	532794	29600	2423	8.2 ± 0.1	171 ± 10	≈ 0

3.2 Distribution of arrival time intervals of recorded air showers

The electronic system installed in the array described can record the arrival time interval between successive air showers. If the arrival time of primary cosmic rays, initiating the air showers, is random, the arrival time of the air showers at the array level should also be random. In this case, the distribution of n-event arrival time intervals for air showers follows the Gamma distribution (Poissonian of order n) [4]. This distribution was invented to predict the waiting time until future events. This is also known as the Erlang(ian) distribution (after the Danish engineer A.K. Erlang, who used it to describe telephone networks).

$$G(t; r, n) = r\frac{(rt)^{n-1}e^{-rt}}{(n-1)!}. \tag{9}$$

Where r is the inverse of the mean value of arrival time interval between two consecutive air shwers (or mean rate of events), and n is the order of the distribution. In case $n = 1$, Equation (9) becomes an exponential function as $G(t; r, 1) = re^{-rt}$. Bhat ([5]) reported that the arrival time interval between air showers did not follow an exponential function but observed two exponential components in the distribution. Subsequent evidence also confirmed this conclusion ([6],[7]). On the other hand, other observations negated that conclusion ([8],[9]). Figure 5 shows the n-event arrival time intervals of air showers observed by our array in case of $n = 1$, 2, and 3 with zenith angle in bins 0°-10°, 10°-20°, 20°-30°, 30°-40°, 40°-50°, and all zenith angles between 0°-60°. Since for the Poisson function of order n, the mean time interval, $\bar{t}_n$, is n/r, and the most probable time interval, $T_{n,p}$, is given by $(n - 1)/ r$, the results are obtained by fitting the Equation (9) with different n(Table 2) is perfectly consistent with the Poisson function and no anomaly are found in this distribution. As expected at each zenith angle interval, the event count rates for the different ns are almost the same. Event count rate is maximized in the zenith range of 20°-30°, which is due to the maximization of the solid angle in this range. The event count rate for all zenith angles obtained by fit is approximately $\simeq 1.8$ counts/min, which is consistent with the value of $r \simeq 1.8$ counts/min stated above. Because $\int_0^\infty x^n e^{-x} dx = n!$, hence the surface of all the curves are the same for different n, and this means that as n increases, the distribution becomes more uniform.

3.3 Effect of environmental parameters on the rate of air shower events

The event rate of air showers depends on some atmospheric parameters, the most important of which are environment pressure and temperature. To investigate these effects, the data of Mehrabad weather station is used.
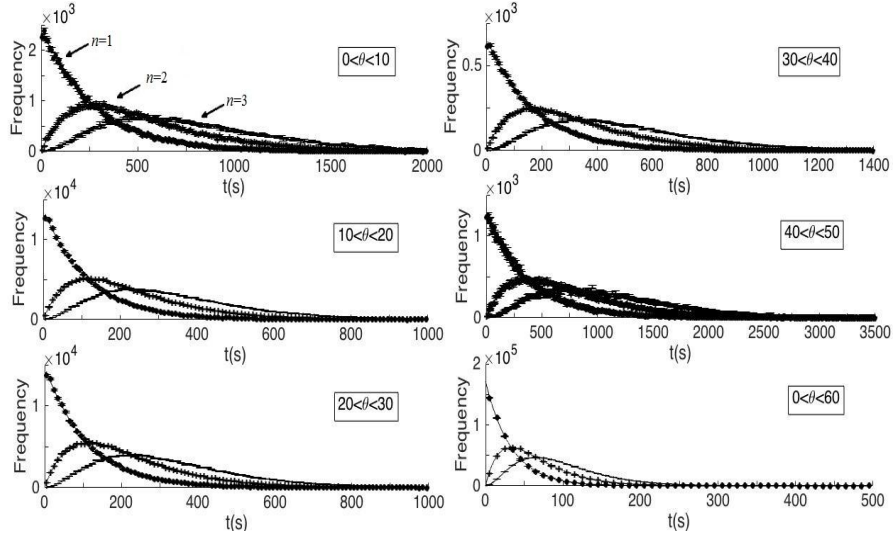
Figure 5: The *n*-event arrival time intervals of air showers in case of *n*= 1, 2, and 3 with different zenith angles. Different *n*s are shown in one of the graphs, top-left, and the rest are similar. Solid curves show the fit of the data with Equation (9).

Table 2: Some parameters of the time interval distributions fitted to the Poisson function of order n, Including count rate, r, mean time interval, $\bar{t}_n$, and most probable time interval, $T_{n,p}$.

Zenith angle		0°-10°	10°-20°	20°-30°	30°-40°	40°-50°	0°-60°
	$n=1$	218±2	515±5	535±4	351±3	159±2	1785±20
$10^3 r \left(\frac{events}{min}\right)$	$n=2$	220±2	520±2	539±2	354±2	159±1	1818±11
	$n=3$	220±1	520±2	540±3	355±2	158±1	1832±3
	$n=1$	459±4	194±2	187±1	285±3	631±7	56±1
$10^2 \bar{t}_n (\min)$	$n=2$	909±6	385±1	371±1	564±4	1260±11	110±1
	$n=3$	1362±8	577±2	556±3	846±4	1894±12	164±1
	$n=1$	0	0	0	0	0	0
$10^2 T_{n,p} (\min)$	$n=2$	455±3	193±1	186±1	282±2	630±6	55±1
	$n=3$	908±5	384±1	371±2	564±3	1263±8	109±1

3.3.1 Pressure effect

Atmospheric pressure affects the recording rate of air showers. This relationship is demonstrated in Figure 6(a).
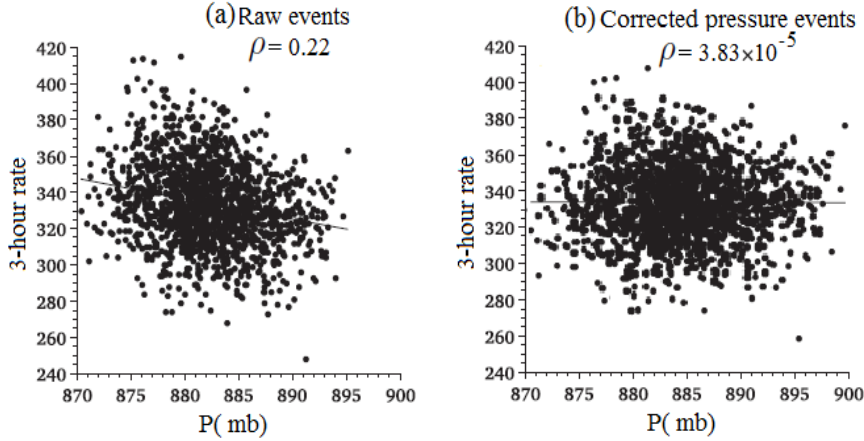

Figure 6: The number of 3-hour events as the environment pressure; (a) raw events, and (b) corrected pressure events. The solid line represents the fitted exponential function.

This figure is a representation of the three-hour rate of events in terms of pressure for angles less than $45°$. This event rate can be modeled with the exponential function $R_P = R_{0P}e^{-\alpha(P-P_0)}$, where R_P is the rate of events at pressure P. The values of R_{0P} and P_0 are calculated from $\frac{1}{N}\Sigma_{k=1}^{N}R_k$ and $\frac{1}{N}\Sigma_{k=1}^{N}P_k$ respectively, where $N = 1711$, which is the number of 3-hour intervals in the experimental data, and R_k and P_k are the recorded count rate and pressure respectively in ith 3-hour interval. The coefficient α is obtained using the least-square method from the following equation.

$$\alpha = -\frac{\Sigma_{k=1}^{N}\ln(\frac{R_k}{R_{0P}})(P_k - P_0)}{\Sigma_{k=1}^{N}(P_k - P_0)^2}. \tag{10}$$

Linear correlation coefficient is given by Pearson's formula.

$$\rho = -\frac{S_{PR}}{\sqrt{S_P S_R}}, \tag{11}$$

where $S_{PR} = \Sigma_{k=1}^{N}\ln(\frac{R_k}{R_{0P}})(P_k - P_0)$, $S_P = \Sigma_{k=1}^{N}(P_k - P_0)^2$, and $S_R = \Sigma_{k=1}^{N}(\ln\frac{R_k}{R_{0P}})^2$. Hence, we have $\alpha = \rho\sqrt{\frac{S_R}{S_P}}$, $\Delta\alpha = \pm\frac{\alpha}{\rho}\sqrt{\frac{1-\rho^2}{N-3}}$. From the data collected from the array, the values of $P_0 \simeq 882\text{mb}$, $R_{0P} \simeq 334/(3 \text{ hours})$, $\alpha \simeq (3.0 + 0.3) \times 10^{-3}/\text{mb}$, and $\rho \simeq 0.22$ are calculated. For the pressure corrected rate, R_P^c, we use the equation $R_P^c = R_m e^{\alpha(P-P_0)}$, where R_m is the measured events rate in the data acquisition. The corrected values R_P^c in terms of atmospheric pressure are shown in Figure 6(b). With this correction, the value of the correlation coefficient changes from $\rho = 0.22$ to $\rho = 3.82 \times 10^{-5}$, which indicates that the data is properly corrected with this method.

3.3.2   Temperature effect

The effect of temperature on the recorded raw event rates can be seen by separating them into different seasons: spring, summer, autumn and winter. The time interval distribution of successive events in different seasons can be seen in Figure 7. These distributions follow the exponential distribution $A\exp(-rt)$, where the values of r (rate of events) for spring, summer, autumn, and winter seasons are 1.78±0.02, 1.74±0.02, 1.76±0.02, and 1.84±0.02 events/min, respectively. One can see this rate decreases with increasing temperature, which indicates that increasing temperature causes changes in air density, and this in turn affects the number of secondary particles in the air shower, resulting in a decrease in the recording of air showers.
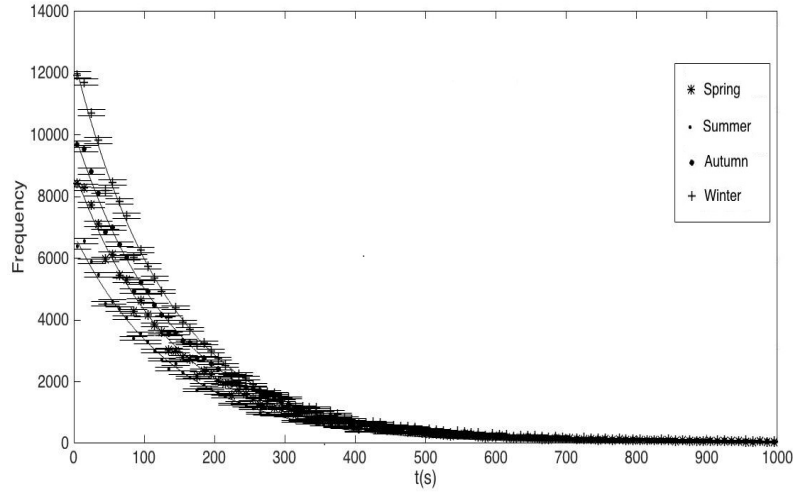

Figure 7: Distribution of successive time intervals of events in different seasons. The curves are fitted with function Ae^{-rt} .

The temperature correction is performed on the values of R_P^c, that is, on the data of Figure 6(b). The method of performing this operation is similar to subsection 3.3.1. It is enough to make the following transformations.

1) $R_k \rightarrow R_{kP}^c$, and $P_k \rightarrow T_k$, $\alpha \rightarrow \beta \simeq (2.0 + 0.1) \times 10^{-3}/°\mathrm{C}$,

2) $R_{0P} \rightarrow R_{0T}$, with $R_{0T} = \frac{1}{N}\Sigma_{k=1}^{N} R_{kP}^c$,

3) $P_0 \rightarrow T_0$, with $T_0 = \frac{1}{N}\Sigma_{k=1}^{N} T_k = 16.7°\mathrm{C}$.

With these transformations, the pressure and temperature corrected event rate with $R_{PT}^c = R_P^c e^{\beta(T-T_0)}$ are calculated. Figure 8 shows the values of R_{PT}^c as a function of temperature. The correlation coefficient after these corrections reaches ρ=-0.008.

3.4   Anisotropy in solar and sidereal time

The number of recorded events, corrected for atmospheric pressure and temperature, in solar and sidereal time is given in Figure 9. With the Fourier analysis up to the first order, given in Section 1-3, the amplitudes and phases and probabilities to get larger values from statistical
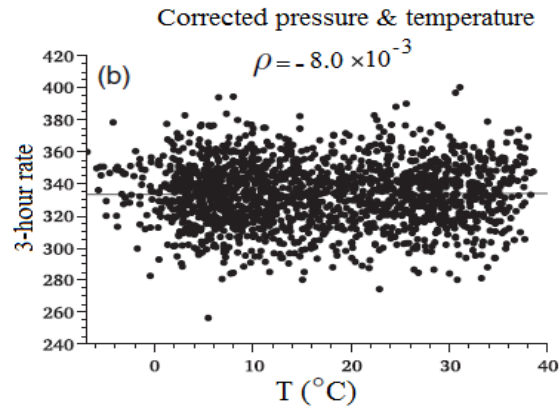
Figure 8: The number of 3-hour events after correcting pressure and temperature.
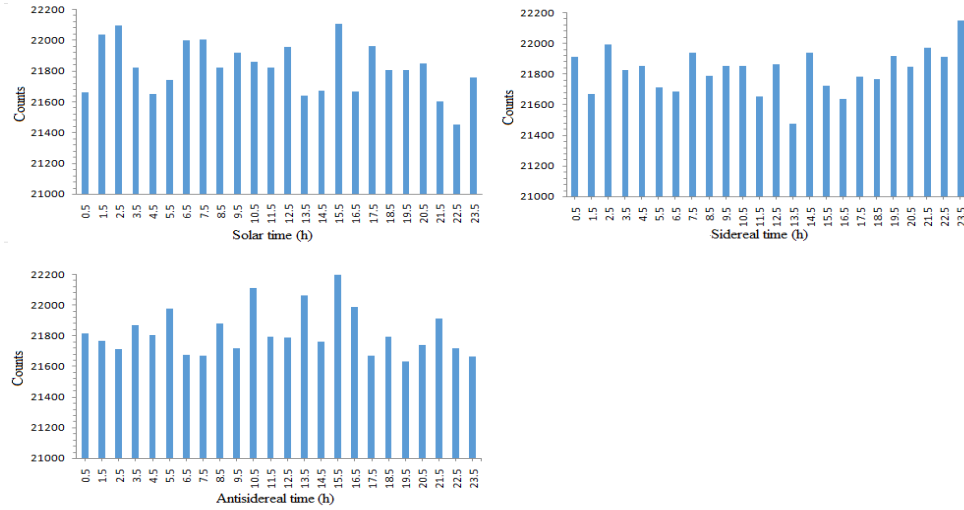

Figure 9: Number of events as a function of solar, sidereal, and antisidereal times, corrected for atmospheric pressure and temperature.

Table 3: Fourier amplitudes and phases at solar, sidereal, and antisidereal times corrected presure and tempereture, and the probabilities to get larger values from statistical fluctuations of an isotropic distribution for each of the 3 time periods.

Period	$\mathcal{N}$	N_0	N_1	$f(\%)$	$\varphi(hours)$	$P(\geq f)$
Solar time	523751	21823	71	0.3 ± 0.04	8.9 ± 0.5	0.25
Sidereal time	523751	21823	91	0.4 ± 0.04	0.2 ± 0.5	0.10
Antisidereal time	523751	21823	80	0.4 ± 0.04	12.8 ± 0.5	0.17

fluctuations of an isotropic distribution for each two time periods are shown in Table 3. One can see that all these amplitudes are consistent with being fluctuations, showing then no signs of remaining systematic effects.

4   Conclusion

During almost one year, more than five hundred thousand cosmic ray events have been registered by an array of 5 scintillator detectors in different directions. With this array, cosmic rays with energies in the range of 30 to 3000 TeV were collected at a rate of 1.8 events per minute. With the time delay of the secondary particles of each air shower, the arrival direction of the primary particle at the top of the atmosphere was calculated using the least square method. The zenith angle of the arrival direction of air showers obeys a $\cos^m\theta$ law with $m= 7.2\pm 0.1$. On the other hand, when an air shower arrives at an angle to the earth's magnetic field, the secondary charged particles in the shower can be deflected. For showers arriving from the north the shower particles have higher deflections than the southern ones of the equal energy with the equal zenith angle. The amplitudes of anisotropy observed in the zenith angle intervals of $0° - 15°$, $15° - 30°$, $30° - 45°$, and $\theta \leq 45°$ are $(6.4 \pm 0.3)\%$, $(8.6 \pm 0.2)\%$, $(16.0 \pm 0.3)\%$, and $(9.9 \pm 0.1)\%$, respectively at the location of Alborz I observatory.

Also, the distribution of one-event, two-event, and three-event arrival time intervals were obtained. With a regression greater than 99.9%, the cosmic ray arrival time distribution agrees with a Poisson distribution function of order n for all n-event arrival time intervals. Using Fourier analysis of data, and considering pressure and temperature corrections, we found no cases that the number of events detected as a function of solar, sidereal, and antisidereal times differ significantly from random expectation, in the energy range of 30 to 3000 TeV.

Acknowledgment

References

[1] Pezeshkian, Y., & et al. 2015, Nucl. Instrum. Methods A, 733, 117.

[2] Mortazavi Moghaddam, S., & Bahmanabadi, M. 2018, PHYSICAL REVIEW D, 97, 062001.

[3] Halataei, S. M. H. M., & et al. 2008, Phys. Rev. D 77, 083001.

[4] Ahlen, S. P., & et al. 1992, Nuclear Physics B, 370, 432.

[5] Bhat, C. L., & et al. 1980, Nature, 288, 146.

[6] Badino, G., & et al. 1980, Lett. Nuovo Cimento, 28, 93.

[7] Katayose, Y., & et al. 1998, IL. Nuovo Cimento, 21, 3.

[8] Smith, G. R., & et al. 1983, Phys. Rev. D, 28, 1601.

[9] Fegan, D. J., & et al. 1981, Proc. XVII ICRC (Paris), 16, 296.